OXFORD

Genome analysis

Somatic selection distinguishes oncogenes and tumor suppressor genes

Pramod Chandrashekar [1,2], Navid Ahmadinejad[1,2], Junwen Wang[1,3], Aleksandar Sekulic[3], Jan B. Egan[3], Yan W. Asmann[4], Sudhir Kumar[5,6], Carlo Maley[2] and Li Liu [1,2,3,*]

[1]College of Health Solutions, Arizona State University, Phoenix, AZ, 85004, USA, [2]Center for Personalized Diagnostics, Biodesign Institute, Arizona State University, Tempe, AZ, 85281, USA, [3]Department of Health Sciences Research & Center for Individualized Medicine, Mayo Clinic Arizona, Scottsdale, AZ, 85259, USA, [4]Department of Health Sciences Research, Mayo Clinic Florida, Jacksonville, AZ, 32224, USA, [5]Institute for Genomics and Evolutionary Medicine, Temple University, Philadelphia, PA, 19122, USA and [6]Department of Biology, Temple University, Philadelphia, PA, 19122, USA

*To whom correspondence should be addressed.

Associate Editor: Russell Schwartz

Abstract

Motivation: Functions of cancer driver genes vary substantially across tissues and organs. Distinguishing passenger genes, oncogenes (OGs) and tumor-suppressor genes (TSGs) for each cancer type is critical for understanding tumor biology and identifying clinically actionable targets. Although many computational tools are available to predict putative cancer driver genes, resources for context-aware classifications of OGs and TSGs are limited.

Results: We show that the direction and magnitude of somatic selection of protein-coding mutations are significantly different for passenger genes, OGs and TSGs. Based on these patterns, we develop a new method (genes under selection in tumors) to discover OGs and TSGs in a cancer-type specific manner. Genes under selection in tumors shows a high accuracy (92%) when evaluated via strict cross-validations. Its application to 10 172 tumor exomes found known and novel cancer drivers with high tissue-specificities. In 11 out of 13 OGs shared among multiple cancer types, we found functional domains selectively engaged in different cancers, suggesting differences in disease mechanisms.

Availability and implementation: An R implementation of the GUST algorithm is available at https://github.com/liliu lab/gust. A database with pre-computed results is available at https://liliulab.shinyapps.io/gust.

Contact: liliu@asu.edu

Supplementary information: Supplementary data are available at *Bioinformatics* online.

1 Introduction

In tumor development, oncogenes (OGs) and tumor-suppressor genes (TSGs) work complementarily to promote and maintain abnormal cell growth (Morris and Chan, 2015; Weinberg, 1994). OGs cause cancers through gain-of-function variants, whereas TSGs operate by loss of function. While there are a few well-known OGs (e.g. *RAS*) and TSGs (e.g. *TP53*), it is fast becoming clear that the tumor-enabling activities of a gene is not the same for all types of cancers. Activities of driver genes depend strongly on their cellular contexts because of tissue-specific organizations of cancer pathways (Schaefer and Serrano, 2016; Schneider *et al.*, 2017; Visvader, 2011). Prediction of functional status of genes in different cancer types and cellular contexts is critical for not only understanding tumor biology, but also informing targeted therapies and drug-repurposing (Morris and Chan, 2015; Schneider *et al.*, 2017; Sleire *et al.*, 2017).

Interestingly, only one computational method (20/20+) are available to predict OGs and TSGs (Tokheim *et al.*, 2016). The 20/20+ is an extension of the 20/20 rule in which OGs have >20% mutations causing missense changes at recurrent positions and TSGs have >20% mutations causing inactivating changes (Vogelstein *et al.*, 2013). However, recurrent missense mutations are not a deterministic feature of OGs because these events can cluster at functionally neutral positions due to high mutational rates (Schaub *et al.*, 2018), and many TSGs harbor hotspots of inactivating missense mutations (Iacobuzio-Donahue *et al.*, 2004; Miller *et al.*, 2015). Meanwhile, random mutational processes may introduce protein-truncating mutations (i.e. nonsense and frame-shifting mutations) into OGs, which increase in frequency via genetic drift with no significant impact on tumor fitness and mislead annotations (Lipinski *et al.*, 2016; Mort *et al.*, 2008; Schaub *et al.*, 2018). Therefore,

conventional ratiometric measures are inadequate to distinguish these two groups of genes.

Because tumor development is an evolutionary process, cells carrying somatic mutations are under natural selection within tumors. The positive selection promotes advantageous genotypes that confer higher fitness to a tumor. The negative selection eliminates genotypes with adverse effects. Neutral evolution lets insignificant genotypes to drift up or down in frequency. In OGs, gain-of-functions may be achieved via missense mutations, which are expected to be positively selected. In contrast, protein-truncating mutations (e.g. nonsense mutations and frame-shifting mutations) often inactivate an OG and are detrimental to tumor fitness, resulting in negative selection. In TSGs, both protein-truncating mutations and missense mutations can be positively selected when they result in the loss of functions. Otherwise, they may drift neutrally or be even under negative selection if they disrupt essential biological functions. For passenger genes (PGs) that do not have significant impact on tumor fitness, we expect that all mutations are under neutral selection (Sun *et al.*, 2017; Williams *et al.*, 2016).

In this study, we tested whether the difference in evolutionary dynamics of missense and truncating mutations has sufficient signal and power to improve the detection of OGs and TSGs beyond that of ratiometric measures. Such contrast is essential to distinguish TSGs deactivated by missense mutations from OGs activated by missense mutations, which is a challenging task for conventional ratiometric measures because hotspots of missense mutations are present in both cases. Furthermore, when activities of a gene vary across cancer types, the direction and magnitude of somatic selection will change accordingly, enabling contextual classification of driver genes.

Our analysis of 10 172 tumor exomes from The Cancer Genome Atlas (TCGA) (Cancer Genome Atlas Research Network *et al.*, 2013) project revealed significant differences in selective patterns of OGs, TSGs and PGs. Based on these patterns, we developed a computational method, named genes under selection in tumors (GUST) that integrates somatic selection of genes in tumor development, molecular conservation during species evolution and conventional ratiometric measures to classify cancer genes in different tissues and organs.

2 Materials and methods

Curation of cancer-type specific functions of driver genes: to test our hypothesis and to train a random forest model, we needed cancer-type specific functional annotations of cancer genes. Because these annotations are not currently available, we conducted manual curations using two lists of genes with complementary information. The first list consisted of 36 OGs, 48 TSGs and 21 genes with dual OG/TSG roles annotated in the cancer gene consensus (CGC, version 87) (Sondka *et al.*, 2018). The tumor-activating or -suppressing roles of these genes have been confirmed with cancer hallmarks in experimental assays and are attributable to coding substitutions or indels (Hanahan and Weinberg, 2000). The second list consisted of 235 computationally predicted driver genes assigned to specific cancer types (Bailey *et al.*, 2018). These predictions were based on a meta-analysis of the TCGA samples with multiple computational programs. These two lists shared 70 genes. We then retrieved somatic mutations of these 70 genes from the TCGA project (Cancer Genome Atlas Research Network *et al.*, 2013). For a gene to qualify as an OG in a specific cancer type, it needs to be annotated as an OG or a dual-role gene in the CGC, predicted as a driver in the meta-analysis of the matching cancer type, and display mutational hotspots in the corresponding TCGA tumor samples. For a gene to qualify as a TSG in a specific cancer type, it needs to be annotated as a TSG or a dual-role gene in the CGC, predicted as a driver in the meta-analysis, and have an overabundance of truncating mutations or missense mutations in the corresponding TCGA tumor samples. For a gene to qualify as a PG in a specific cancer type, it needs to be predicted as a PG in the meta-analysis and shows no mutational hotspots or overabundance of truncating mutations in corresponding TCGA tumor samples. Genes that did not meet these requirements

were removed. The final collection consisted of 55 OG annotations, 174 TSG annotations and 304 PG annotations that involved a total of 50 known driver genes and 33 cancer types (Supplementary Table S1).

Somatic selection features: given a gene with somatic mutations reported in a collection of tumor samples, we denote the selection coefficient of missense mutations as ω, and the selection coefficient of protein-truncating (nonsense and frame-shifting) mutations as φ. To account for differences in mutational rates, we consider seven substitution types (1: A→C or T→G, 2: A→G or T→C, 3: A→T or T→A, 4: C→A or G→T, 5: C→G or G→C, 6: C→T or G→A at non-CpG sites, and 7: C→T or G→A at CpG sites), one insertion type and one deletion type. Based on the statistical framework proposed by Greenman *et al.* (2006), the probability of observing these mutations is a product of multinomial distributions

$$L(\{s_k, m_k, n_k, i_k, f_k\}_k) = \prod_k \frac{t_k!}{s_k! m_k! n_k! i_k! f_k!} \frac{(S_k)^{s_k}(\omega M_k)^{m_k}(\varphi N_k)^{n_k}(I_k)(\varphi F_k)^{f_k}}{(S_k + \omega M_k + \varphi N_k + I_k + \varphi F_k)^{t_k}}$$
(1)

where s_k, m_k, n_k, i_k and f_k are the observed numbers of synonymous, missense, nonsense, in-frame indel and frame-shifting indel mutations in the kth rate category, respectively; S_k, M_k, N_k, I_k and F_k are the corresponding expected numbers of changes computed by saturated mutations, in which we introduced each possible single nucleotide mutation one at a time; and $t_k = s_k + m_k + n_k + i_k + fk$ is the total number of observed mutations. The values of $\log(\omega)$ and $\log(\varphi)$ are determined by maximizing the log likelihood L and constrained within the range of $[-5, 5]$. The sign and absolute value of $\log(\omega)$ and $\log(\varphi)$ indicate the direction and magnitude of somatic selection. Values around 0 indicate neutral somatic evolution. Details of parameter tuning are available in Supplementary Methods and Supplementary Figure S1.

GUST algorithm: GUST is a random forest model that predicts the class label (OG, TSG or PG) of a gene based on 10 features (Supplementary Table S2 and Fig. S2). In addition to the $\log(\omega)$ and $\log(\varphi)$ values, we also compute ratiometric measures to detect mutational hotspots and conservational measures to estimate substitutional rate across species. Specifically, given a gene and a set of somatic missense mutations detected in tumor samples, we applied density estimates with a rectangular kernel and a bandwidth of five protein positions to aggregate closely-spaced mutations into peaks and denoted the highest peak as the summit. To estimate evolutionary conservation of a gene, we downloaded multiple sequence alignments of 100 vertebrate species from the UCSC Genome Browser (Kent *et al.*, 2002), and computed the substitution rate of each protein position (Kumar *et al.*, 2012; Liu and Kumar, 2013). The average substitution rate over all positions measures the gene-level conservation. The average substitution rate over positions in a summit measures the conservation of a mutational hotspot. For a given gene/cancer-type pair in the curated annotations, we retrieved somatic mutations from the corresponding TCGA tumor samples and computed values of the 10 features. Using these training data, we constructed a random forest classifier with 200 trees. For each gene, this model produces three probability scores of it being an OG, a TSG or a PG, respectively. It assigns the class label based on the highest probability score. For all predictions, GUST reports random forests probability score, sensitivity and specificity. For OG or TSG predictions, GUST also reports false discovery rate. Detailed information of data processing, feature selection and false discovery rate calculation is available in the Supplementary Materials.

3 Results

3.1 Different selection patterns of cancer genes

For each gene/cancer-type pair in our manual annotations, we retrieved somatic mutations in the matching tumor samples from the TCGA project, and computed the somatic selection coefficients. We found that missense mutations in OGs were under stronger positive selection than in TSGs, as the mean $\log(\omega)$ was 4.18 and 1.68, respectively ($P < 10^{-10}$, Fig. 1A). In contrast, protein-truncating
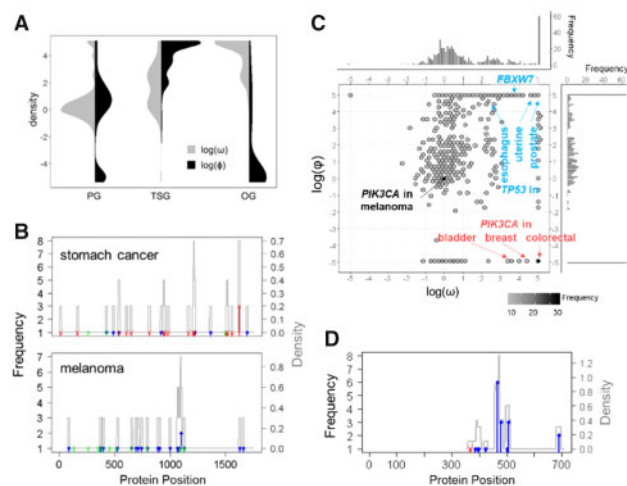
Fig. 1. The distribution of selection coefficients of the curated genes. (**A**) Split violin plot showing densities of $\log(\omega)$ and $\log(\varphi)$ values for PGs, TSGs and OGs. (**B**) Positional distribution of somatic mutations of the *BCOR* gene in stomach cancer and in melanoma. Vertical lines represent frequencies of various types of mutations at a given position. Synonymous, missense and truncating mutations are represented by green, blue and red lines, respectively. Gray lines are density curves. (**C**) Scatter plot of $\log(\omega)$ and $\log(\varphi)$ values. Shades of hexagon bins represent the number of observations. (**D**) Positional distribution of somatic mutations of the *FBXW7* gene in uterine carcinosarcoma. (Color version of this figure is available at *Bioinformatics* online.)

Table 1. Performance of GUST and 20/20+

		Binary classes			Three classes
	Positive	OG, TSG	OG	TSG	
	Negative	PG	PG, TSG	PG, OG	
GUST	TPR	0.93	0.84	0.93	—
	TNR	0.94	0.98	0.95	—
	PPV	0.92	0.85	0.9	—
	NPV	0.95	0.98	0.96	—
	ACC	0.94	0.97	0.94	0.92
	AUC	0.97	0.99	0.97	0.98[a]
20/20+	TPR	0.90	0.95	0.86	—
	TNR	0.85	0.97	0.90	—
	PPV	0.82	0.78	0.81	—
	NPV	0.92	0.99	0.93	—
	ACC	0.88	0.97	0.89	0.86
	AUC	0.94	0.97	0.93	0.95[a]

[a]Macro-AUC values were calculated by averaging three one-vs-rest ROC curves. Linear interpolation was used between points of ROC (Wei and Wang, 2018).

TPR, true positive rate, sensitivity; TNR, true negative rate, specificity; PPV, positive predictive value, precision; NPV, negative predictive value; ACC, accuracy; AUC, area under the ROC curve.

mutations showed positive selection in TSGs [mean $\log(\varphi) = 4.08$)], but negative selection in OGs [mean $\log(\varphi) = -3.25$, respectively)]. The effect size of the differences observed is very large, and the *P*-values highly significant ($P < 10^{-8}$). The selection measures observed on PGs were close to zero [mean $\log(\omega) = 0.60$ for missense and mean $\log(\varphi) = -0.28$ for nonsense mutations]. Therefore, TSGs, OGs and PGs show significant evolutionary differences.

The distribution of $\log(\varphi)$ values of PGs had two peaks. The largest peak located close to 0, consistent with the expected neutral selection of PGs. The second peak located close to –5, indicating that loss of function of these PGs is detrimental to tumor growth. Interestingly, many genes in the second peak are established TSGs in other cancer types where loss of their functions is beneficial to tumors. For example, the *BCOR* gene regulates apoptosis in stomach cancer and had overabundant truncating mutations (Cancer Genome Atlas Research Network, 2014). However, this gene was depleted of truncating mutations in melanoma (Fig. 1B). Such contrast suggested that although disabled TSGs promote tumor growth in certain cellular contexts, maintaining their activities may be essential for tumor development in other contexts. We then examined the joint distributions of $\log(\omega)$ and $\log(\varphi)$ values and found that somatic selection patterns reflected the contextual activities of a gene (Fig. 1C). For example, the *PIK3CA* gene had high $\log(\omega)$ values and low $\log(\varphi)$ values in bladder cancers, breast cancers and colorectal cancers, consistent with its well-known OG role. The $\log(\omega)$ and $\log(\varphi)$ values of this gene were close to zero in melanoma, indicating lack of a role resulting in neutral patterns. Recently, the passenger role of *PIK3CA* in melanoma has been proposed in a study that shows *PIK3CA*-mutated melanoma cells rely on cooperative signaling to promote cell proliferation and PI3K inhibitors do not repress tumor growth in the absence of other activating driver genes in melanoma (Silva *et al.*, 2017).

For TSGs, such as *TP53*, their high $\log(\varphi)$ values occupied spaces distant from OGs in the distribution plot (Fig. 1C). As discussed earlier, TSGs with hotspots of missense mutations, such as the *FBXW7* gene in uterine carcinosarcoma (Fig. 1D) are challenging to distinguish from OGs using ratiometric methods. Based selection measures [$\log(\omega)=5.0$, $\log(\varphi) =3.9$], this gene is unambiguously separated from OGs [$\log(\varphi)\ll 0$], consistent with our expectations.

3.2 Performance of the GUST method

We trained a random forest classifier (GUST) using the 10 features of the curated genes. Via 10-fold gene-holdout cross-validations, the testing accuracy of GUST was 0.92. As a comparison, the accuracy of 20/20+ on the entire training dataset was 0.86. To calculate traditional performance metrics, we converted three-class predictions to binary predictions by contrasting one class with the other two classes combined, i.e. one-vs-rest predictions. In all categories, GUST showed better or comparable performance than 20/20+. The largest improvements were on the precision of identifying OGs and TSGs, which increased from 0.78–0.82 in 20/20+ to 0.85–0.92 in GUST (Table 1). The receiver operating characteristic (ROC) curves reconfirmed the superior performance of GUST (Fig. 2A). Compared to 20/20+, GUST had a significantly higher area under the curve (AUC) value of the PG-vs-rest ROC curve (0.97 versus 0.94, DeLang's test $P = 0.0008$), and a significantly higher AUC value of the TSG-vs-rest ROC curve (0.97 versus 0.93, $P = 0.001$). However, the AUC values of the OG-vs-rest ROC curves were not significantly different between these two methods (0.99 versus 0.97, $P = 0.21$).

To evaluate the concordance of GUST classifications with other methods that predict cancer drivers but do not distinguish OGs and TSGs, we computed a driver score by adding the OG and TSG scores of each gene. The TCGA PancanAtlas consortium reported a collection of putative driver genes based on consensus predictions from 12 computational methods (Bailey *et al.*, 2018). We first examined the 510 gene/cancer-type pairs (204 unique genes) predicted as drivers by ≥2 methods. In this permissive list, GUST predicted 373 pairs (73.1%, 145 unique genes) as drivers. We then examined the 283 gene/cancer-type pairs (109 unique genes) predicted as drivers by ≥3 methods. In this more stringent list, GUST predicted 254 pairs (89.8%, 96 unique genes) as drivers. These results showed that drivers predicted by GUST had a high agreement with existing methods while providing additional OG/TSG classifications.

To measure the importance of each predictor in the random forest model, we computed the mean decreased Gini index by permuting out-of-bag samples (Louppe *et al.*, 2013). The most informative predictors are the selection coefficients and fraction of truncating mutations, followed by the selection coefficient and fraction of missense mutations (Fig. 2B). Interestingly, evolutionary conservation was not very informative, which may be because a vast majority of drivers are known to occur at highly conserved positions
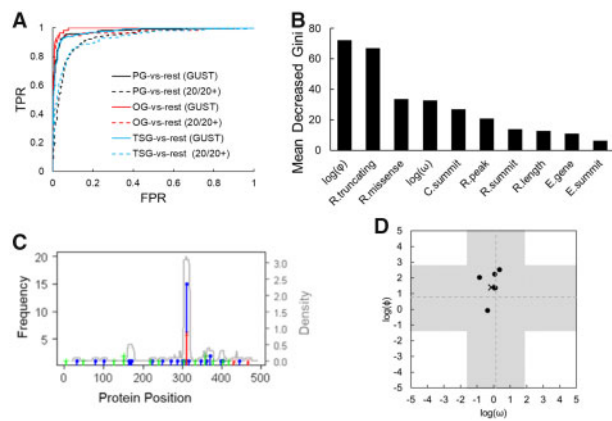
Fig. 2. The GUST method. (**A**) ROC curves of one-vs-rest predictions for GUST and for 20/20+. (**B**) Variable importance of each feature in the random forest model. (**C**) Positional distribution of somatic mutations of the *MB21D2* gene. Mutations were combined from tumor samples of bladder cancer, cervical cancer, head and neck cancer, lung adenocarcinoma and lung squamous cell carcinoma. A mutation hotspot is located at coding position 931 that corresponds to protein position 311. (**D**) Selection coefficients estimated for the *MB21D2* gene in individual cancer types (dots) and for combined samples (cross). Broken lines are the mean selection coefficient of all genes analyzed using all TCGA samples. Shaded areas are the 95% confidence intervals of the mean selection coefficients

(Dudley *et al.*, 2012), providing a limited power to discriminate OGs and TSG.

Although recurrence among patients has been taken as a surrogate of mutations under functional selection, recent investigations have shown that passenger hotspot mutations are common (Buisson *et al.*, 2019; Hess *et al.*, 2019). For example, multiple samples of various cancer types harbored a C->T or C->G mutation at position 931 of the *MB21D2* gene (Fig. 2C, Supplementary Fig. S3). Buisson *et al.* discovered that this mutational hotspot is due to its location in a hairpin loop susceptible to mutagenesis and functions as a passenger (Buisson *et al.*, 2019). GUST analysis confirmed that the selection pattern of this gene was consistent with neutral evolution in individual cancer types and in the combined samples (Fig. 2D). Thus, GUST predicted the *MB21D2* gene as a PG correctly. This demonstrated the effectiveness of quantifying the contribution of genetic alterations to tumor fitness in cancer gene classifications.

3.3 Application to TCGA data

We retrieved somatic mutations from whole-exome sequencing data of 10 172 TCGA tumor samples spanning 33 cancer types. We then removed low-quality mutations, hyper-mutated or hypo-mutated samples, genes with fewer than four protein-altering mutations and genes mutated in <2% of tumors (Supplementary Materials). We applied GUST to the remaining 9663 samples. We predicted 161 OGs of which 98 were unique genes in 29 cancer types. We also predicted 331 TSGs of which 179 were unique genes in 33 cancer types (Fig. 3A, Supplementary Tables S3 and S4).

3.3.1 Novel driver genes

The GUST-predicted drivers consisted of 55 putative OGs and 97 putative TSGs that were classified as PGs in the CGC database (Sondka *et al.*, 2018). Most (81.7%) of these new putative drivers were annotated in only one cancer type and had low probability scores. To estimate the confidence of each prediction, we computed the sensitivity and specificity of each one-vs-rest prediction based on the ROC curves. We then derived a list of high-confidence drivers consisting of 22 OGs with OG-vs-rest specificity ≥0.99 and 74 TSGs with TSG-vs-rest specificities ≥0.99, all of which had a PG-vs-rest sensitivity ≥0.99. This short list of high-confidence drivers included two novel OGs and 28 novel TSGs not annotated in the CGC. The two novel OGs (*CNOT9* in melanoma and *GTF2I* in thymoma) had single mutational hotspots disrupting highly
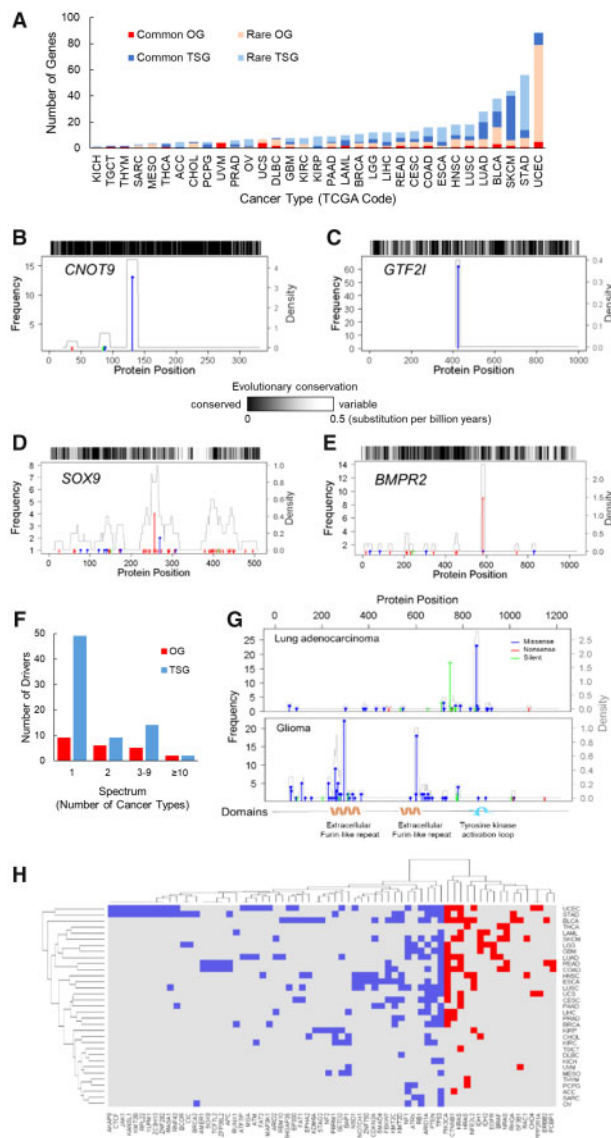

Fig. 3. GUST analysis of the TCGA samples. (**A**) Number of common and rare OGs and TSGs found in each cancer type. Abbreviations of cancer types are listed in Supplementary Table S3. (**B–E**) Positional distributions of somatic mutations in novel OGs and TSGs. Evolutionary conservation of each position, measured as number of substitutions per billion years is displayed above each plot. (**F**) Distribution of driver genes with different spectrum of tissue specificity. (**G**) Positional distribution of mutations in the *EGFR* gene in lung adenocarcinoma and glioma (low-grade glioma and glioblastoma combined). (**H**) Two-way clustering of driver genes and cancer types. Driver genes found in more than one cancer type are used (OGs in red and TSGs in blue). (Color version of this figure is available at *Bioinformatics* online.)

conserved protein positions (Fig. 3B and C). The *GTF2I* mutant stimulates cell proliferation *in vitro* and has been associated with favorable prognosis of thymoma (Roy, 2017).

All of the novel TSGs had an overabundance of truncating mutations (Supplementary Fig. S4). For example, frame-shifting mutations in *SOX9* were observed in 40 colon cancers (Fig. 3D). As an atypical tumor suppressor, *SOX9* has been shown to interact with nuclear β-catenin. Inactivation of *SOX9* causes loss of inhibition of the oncogenic Wnt/β-catenin signaling pathway and is associated with patient survivals (Prevostel *et al.*, 2016). Some novel TSGs harbor mutational hotspots. For instance, the N583fs frame-shifting mutation in *BMPR2* introduced premature stops of protein synthesis and was observed in nine stomach adenocarcinomas (Fig. 3E). We

searched the literature and found supporting evidence of the tumor suppressing functions of 22 (78.6%) novel TSGs (Supplementary Table S5). Many of these novel TSGs were also annotated as putative drivers by other computational methods (Bailey *et al.*, 2018).

As an independent assessment of the validity of these predicted drivers, we examined how many of their mutations were in major clones and compared with PGs. The rationale is that genes frequently mutated in sub-clones may not suggest a selective advantage, but rather other mechanisms, such as increased background mutational rates. Specifically, we used SciClone (Miller *et al.*, 2014) to cluster mutations in each tumor based on variant allele frequencies. We considered the cluster with the highest variant allele frequencies as the major clone and the remaining clusters as sub-clones. For the 30 novel drivers, 93.2% of protein-altering mutations were in major clones, which was similar to the percentage (93.7%) for the 96 known drivers (Fisher's exact test $P = 0.54$). For the 40 most frequently mutated PGs, a significantly lower percentage (89.9%) of protein-altering mutations were in major clones (Fisher's exact test $P = 10^{-4}$). Therefore, these predicted drivers highly likely promote tumorigenesis.

3.3.2 Spectrum of tissue specificity

Even after removing low-confidence predictions, most of the drivers annotated by GUST were engaged in only one cancer type, showing high tissue-specificities. Only 13 (59.1%) OGs and 25 (33.8%) TSGs in this high-confidence set are broad-spectrum drivers, promoting tumorigenesis in two or more cancer types (Fig. 3F). The most prevalent OG was the *PIK3CA* gene found in 15 cancer types with high confidence, followed by the *KRAS/NRAS/HRAS* genes found in 13 cancer types. The most prevalent TSG was the *TP53* gene found in 18 cancer types, followed by the *ARID1A* gene found in 10 cancer types.

Furthermore, 11 out of the 13 broad-spectrum OGs possessed multiple hotspots (one-sided proportional test $P < 0.05$ after Bonferroni corrections, Supplementary Fig. S5 and Supplementary Methods). For each significant hotspot, we examined the affected functional domains as annotated in the NCBI Gene database. A representative example is the *EGFR* gene. In lung adenocarcinoma, 48% of missense mutations clustered at a single mutational hotspot affecting the tyrosine kinase activation loop (Fig. 3G). In glioma, only one mutation hit this loop (chi-square test $P < 10^{-18}$), and 69.3% of all missense mutations clustered at two hotspots affecting the extracellular domains independent of kinase activities. The contextual selection of mutations averting the kinase catalytic domain in glioma suggests an alternate path of activating *EGFR* signaling. In fact, several studies have reported the associations of these hotspot mutations with different levels of *EGFR* activities (Kamburov *et al.*, 2015; Niu *et al.*, 2016; Porta-Pardo *et al.*, 2017). For cancer management, although tyrosine kinase inhibitors blocking *EGFR* are common in the therapeutic armamentarium of lung cancer (Grigoriu *et al.*, 2015; Takeda and Nakagawa, 2019), these agents have not been successful in treating glioma even with improved drug delivery techniques to penetrate the blood–brain barrier (Bethune *et al.*, 2010; Vivanco *et al.*, 2012; Westphal *et al.*, 2017). These findings suggest a potential direction to investigate and enhance current treatment regimen.

Interestingly, each of the 33 cancer types engaged at least one broad-spectrum driver and multiple tissue-specific drivers, implicating the synchrony of convergent and divergent disease pathways. Clustering of cancers based on broad-spectrum driver genes grouped cancer types largely matching their tissue and cellular origins (Fig. 3H).

4 Discussions

Distinguishing OGs and TSGs in individual cancer types is critical to understanding cancer etiology and pinpointing clinically actionable targets. In this study, we proved that protein-coding mutations in OGs and TSGs are under different somatic selection, and subsequently developed the GUST method to discover cancer-type specific functions of cancer driver genes. We compared GUST with the 20/20+ method that is the only available method to classify OGs and

TSGs. Both GUST and 20/20+ employ a random forest model to integrate features extracted from tumor exomes. Despite that GUST uses only 10 features compared to 24 features in 20/20+, the accuracy of GUST is consistently higher. In the GUST model, selection measures contribute the most information content. In 20/20+, the *P*-value of enrichment of inactivating mutations is the most informative feature. Interestingly, this feature is also related to selection, although it is not a strict evolutionary measure (Kryazhimskiy and Plotkin, 2008; Temko *et al.*, 2018). These results suggest that using a small number of features engineered on evolutionary mechanisms is more powerful than feeding a large number of raw features to machine learning models. Furthermore, given the scarcity of known drivers for specific cancer types, reducing the number of features in predictive models helps mitigate overfitting problems.

We acknowledge that a driverMAPS (Zhao *et al.*, 2019) method has been recently developed that estimates selection coefficients of a gene under three competing models (i.e. a PG, an OG and a TSG model). However, this method later combines the OG model and the TSG model into a driver model and contrasts it with the PG model to predict driver genes. Consequently, the reported posterior likelihood and false discovery rate are for the purpose of distinguishing drivers and passenger, but not OGs versus TSGs. Via personal communications with the authors of driverMAPS, we confirmed that this method does not provide statistical significance of OG and TSG classifications. Therefore, we did not compare GUST with driverMAPS.

While we discovered many known and novel cancer driver genes, none of them showed dual OG/TSG roles with high confidence in our analysis. A straightforward explanation is that GUST makes predictions based on protein-altering substitutions and indels, thus it is unable to capture genes acting through other mechanisms, such as noncoding regulatory variants, copy number variants, translocations, fusions, differential expressions, post-translational modifications and epigenetic regulations. Further investigations will shed light on key switches that divert paths of dual-role drivers. We also note that genes with only a small number of mutations may cause non-convergence problems during maximum likelihood estimations of selection coefficients, which limits the application of GUST to discovering rare drivers.

For practical use, we have built an online database (https://liliu lab.shinyapps.io/gust) with pre-computed results of analyzing TCGA samples. Users can query the database and visually inspect somatic selection patterns and conservational patterns of selected genes. Combined with information showing if a gene has been annotated by CGC as a driver or a drug target, users can make informed decisions on prioritizing candidate genes for further investigations. The R implementation of the GUST algorithm is available on Github (https://github.com/liliulab/gust).

5 Conclusions

Somatic selection is a quantitative measure of the impact of mutated genes on tumor fitness. The GUST method estimates these features directly from whole-exome sequencing or targeted sequencing data and pinpoints to genes and functional domains driving tumorigenesis in different cellular contexts. As gene-centered treatment and drug-repurposing attracts increasing interest, we expect this new method and the online database will facilitate discoveries of clinically actionable targets.

References

Bailey,M.H. *et al.* (2018) Comprehensive characterization of cancer driver genes and mutations. *Cell*, **173**, 371–385.

Bethune,G. *et al.* (2010) Epidermal growth factor receptor (EGFR) in lung cancer: an overview and update. *J. Thorac. Dis.*, **2**, 48–51.

Buisson,R. *et al.* (2019) Passenger hotspot mutations in cancer driven by APOBEC3A and mesoscale genomic features. *Science*, **364**, eaaw2872.

Cancer Genome Atlas Research Network. (2014) Comprehensive molecular characterization of gastric adenocarcinoma. *Nature*, **513**, 202–209.

Cancer Genome Atlas Research Network *et al.* (2013) The Cancer Genome Atlas Pan-Cancer analysis project. *Nat. Genet.*, **45**, 1113–1120.

Dudley,J.T. *et al.* (2012) Human genomic disease variants: a neutral evolutionary explanation. *Genome Res.*, **22**, 1383–1394.

Greenman,C. *et al.* (2006) Statistical analysis of pathogenicity of somatic mutations in cancer. *Genetics*, **173**, 2187–2198.

Grigoriu,B. *et al.* (2015) Management of EGFR mutated nonsmall cell lung carcinoma patients. *Eur. Respir. J.*, **45**, 1132–1141.

Hanahan,D. and Weinberg,R.A. (2000) The hallmarks of cancer. *Cell*, **100**, 57–70.

Hess,J.M. *et al.* (2019) Passenger hotspot mutations in cancer. *Cancer Cell*, **36**, 288–301.

Iacobuzio-Donahue,C.A. *et al.* (2004) Missense mutations of MADH4: characterization of the mutational hot spot and functional consequences in human tumors. *Clin. Cancer Res.*, **10**, 1597–1604.

Kamburov,A. *et al.* (2015) Comprehensive assessment of cancer missense mutation clustering in protein structures. *Proc. Natl. Acad. Sci. USA*, **112**, E5486–E5495.

Kent,W.J. *et al.* (2002) The human genome browser at UCSC. *Genome Res.*, **12**, 996–1006.

Kryazhimskiy,S. and Plotkin,J.B. (2008) The population genetics of dN/dS. *PLoS Genet.*, **4**, e1000304.

Kumar,S. *et al.* (2012) Evolutionary diagnosis method for variants in personal exomes. *Nat. Methods*, **9**, 855–856.

Lipinski,K.A. *et al.* (2016) Cancer evolution and the limits of predictability in precision cancer medicine. *Trends Cancer*, **2**, 49–63.

Liu,L. and Kumar,S. (2013) Evolutionary balancing is critical for correctly forecasting disease-associated amino acid variants. *Mol. Biol. Evol.*, **30**, 1252–1257.

Louppe,G. *et al.* (2013) Understanding variable importances in forests of randomized trees. In: *Advances in Neural Information Processing Systems*, pp. 431–439.

Miller,C.A. *et al.* (2014) SciClone: inferring clonal architecture and tracking the spatial and temporal patterns of tumor evolution. *PLoS Comput. Biol.*, **10**, e1003665.

Miller,M.L. *et al.* (2015) Pan-cancer analysis of mutation hotspots in protein domains. *Cell Syst.*, **1**, 197–209.

Morris,L.G. and Chan,T.A. (2015) Therapeutic targeting of tumor suppressor genes. *Cancer*, **121**, 1357–1368.

Mort,M. *et al.* (2008) A meta-analysis of nonsense mutations causing human genetic disease. *Hum. Mutat.*, **29**, 1037–1047.

Niu,B. *et al.* (2016) Protein-structure-guided discovery of functional mutations across 19 cancer types. *Nat. Genet.*, **48**, 827–837.

Porta-Pardo,E. *et al.* (2017) Comparison of algorithms for the detection of cancer drivers at subgene resolution. *Nat. Methods*, **14**, 782–788.

Prevostel,C. *et al.* (2016) SOX9 is an atypical intestinal tumor suppressor controlling the oncogenic Wnt/ss-catenin signaling. *Oncotarget*, **7**, 82228–82243.

Roy,A.L. (2017) Pathophysiology of TFII-I: old guard wearing new hats. *Trends Mol. Med.*, **23**, 501–511.

Schaefer,M.H. and Serrano,L. (2016) Cell type-specific properties and environment shape tissue specificity of cancer genes. *Sci. Rep.*, **6**, 20707.

Schaub,F.X. *et al.* (2018) Pan-cancer alterations of the MYC oncogene and its proximal network across the Cancer Genome Atlas. *Cell Syst.*, **6**, 282–300.

Schneider,G. *et al.* (2017) Tissue-specific tumorigenesis: context matters. *Nat. Rev. Cancer*, **17**, 239–253.

Silva,J.M. *et al.* (2017) PIK3CA-mutated melanoma cells rely on cooperative signaling through mTORC1/2 for sustained proliferation. *Pigment Cell Melanoma Res.*, **30**, 353–367.

Sleire,L. *et al.* (2017) Drug repurposing in cancer. *Pharmacol. Res.*, **124**, 74–91.

Sondka,Z. *et al.* (2018) The COSMIC Cancer Gene Census: describing genetic dysfunction across all human cancers. *Nat. Rev. Cancer*, **18**, 696–705.

Sun,R. *et al.* (2017) Between-region genetic divergence reflects the mode and tempo of tumor evolution. *Nat. Genet.*, **49**, 1015–1024.

Takeda,M. and Nakagawa,K. (2019) First- and second-generation EGFR-TKIs are all replaced to osimertinib in chemo-naive EGFR mutation-positive non-small cell lung cancer? *Int. J. Mol. Sci.*, **20**, E146.

Temko,D. *et al.* (2018) The effects of mutational processes and selection on driver mutations across cancer types. *Nat. Commun.*, **9**, 1857.

Tokheim,C.J. *et al.* (2016) Evaluating the evaluation of cancer driver genes. *Proc. Natl. Acad. Sci. USA*, **113**, 14330–14335.

Visvader,J.E. (2011) Cells of origin in cancer. *Nature*, **469**, 314–322.

Vivanco,I. *et al.* (2012) Differential sensitivity of glioma- versus lung cancer-specific EGFR mutations to EGFR kinase inhibitors. *Cancer Discov.*, **2**, 458–471.

Vogelstein,B. *et al.* (2013) Cancer genome landscapes. *Science*, **339**, 1546–1558.

Wei,R. and Wang,J. (2018) Package 'multiROC'. Release 1.1.1. version 1.1.1. https://cran.r-project.org/web/packages/multiROC/index.html (17 April 2019, date last accessed).

Weinberg,R.A. (1994) Oncogenes and tumor suppressor genes. *CA Cancer J. Clin.*, **44**, 160–170.

Westphal,M. *et al.* (2017) EGFR as a target for glioblastoma treatment: an unfulfilled promise. *CNS Drugs*, **31**, 723–735.

Williams,M.J. *et al.* (2016) Identification of neutral tumor evolution across cancer types. *Nat. Genet.*, **48**, 238–244.

Zhao,S. *et al.* (2019) Detailed modeling of positive selection improves detection of cancer driver genes. *Nat. Commun.*, **10**, 3399.